A Biofluidic Random Laser Cytometer for Biophysical Phenotyping of Cell Suspensions

Jijun He[a†], Shuhuan Hu[bc†*], Jifeng Ren[b], Xin Cheng[a], Zhijia Hu[de], Ning Wang[f], Huangui Zhang[c], Raymond H. W. Lam[b], Hwa-Yaw Tam[a]

[a] Department of Electrical Engineering, The Hong Kong Polytechnic University, Kowloon, Hong Kong, China

[b] Department of Mechanical and Biomedical Engineering, City University of Hong Kong, Kowloon, Hong Kong, China

[c] BGI-Shenzhen, Shenzhen, Guangdong, China

[d] School of Instrument Science and Opto-Electronics Engineering, Hefei University of Technology, Hefei 230009, China

[e] Aston Institute of Photonic Technologies, Aston University, Birmingham B4 7ET, UK

[f] National Engineering Laboratory for Fiber Optic Sensing Technology, Wuhan University of Technology, Wuhan, China

† these authors contributed equally to this work

* correspondence should be addressed to shuhuanhu2-c@my.cityu.edu.hk

Sensitivity analysis

According to Equation 3 in the main text, the scattering mean free path l_s is influenced by cell refractive index n, cell diameter d and cell concentration ρ. The influences of these three parameters could be determined by standard sensitivity analysis. The sensitivity of the three parameters are:

$$\frac{\Delta l_s}{l_s} = \frac{-12n^2}{(n^2+2)(n^2-1)} \times \frac{\Delta n}{n} \approx -70.6\frac{\Delta n}{n}$$

$$\frac{\Delta l_s}{l_s} = -6\frac{\Delta d}{d}$$

$$\frac{\Delta l_s}{l_s} = -\frac{\Delta \rho}{\rho}$$

Usually, the variation of refractive index of different cell types is usually 0.15% ~0.80%[1], which contributes to the variation of scattering mean free path by 10.6% ~ 56.5%;

The variation of the cell diameter between the normal cell MCF-10A and cancerous cells (MCF-7 and MDA-MB-231) is 42.9%, which contributes to the variation of the scattering mean free path by 257%;

The accuracy of our cell counting method is ~2%[2], which contributes to the variation of the scattering mean free path by 2%.

We can see that the cell diameter and the cell refractive index are the main contributors to the variations of the scattering properties. And the error induced by the cell counting could be neglected.

The influences of cell density on the random laser properties

To investigate the influence of cell density on the laser threshold, we carried out the experiment with cell density varied from 7×10^3 cells/ml to 8×10^7 cells/ml, as shown in Figure S1. The threshold of the BFRL with different types of cells all show sustained reduction as the cell density increases. Similar density dependent threshold variation has been reported in previous studies.[3–5] This phenomenon can be explained as following. When the cell density is low (i.e. low scattering strength), the system is operated in the weakly diffusion region and the optical feedback provided by the system is too low to form effective laser cavity. In this case, the emission spectra are mainly manifest as ASE or incoherent random laser. With the increasement of the cell density, the optical feedback gradually becomes strong enough to form several laser cavities with sufficient quality factor. Accordingly, the laser threshold is decreased, and discrete sharp peaks emerges on the top of the emission spectra. However, when the cell density becomes larger than 10^7 cells/ml, the increasement of the cell density will not significantly reduce the lasing threshold. This is because the cells with large density forms numerous laser cavities, which cause the strong mode competition and consume large pump energy. In our study, the cell density is set to be 2×10^6 cells/ml. Under this cell density, the laser threshold values are low and the differences between the laser threshold values of the BFRL with different cell types are distinct.

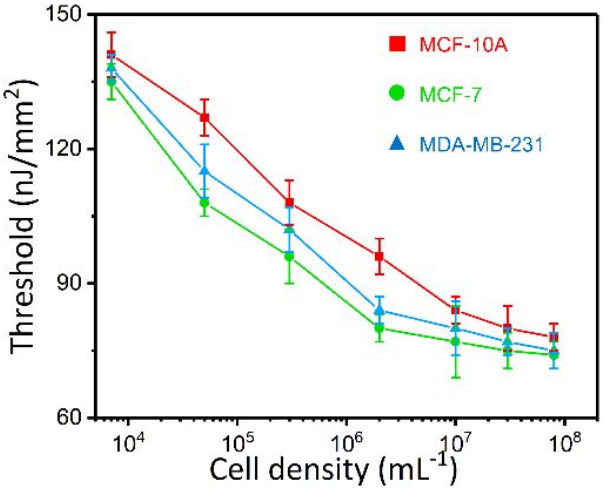

Figure S1. The threshold values of the BFRL devices as a function of the cell density.

Repeatability and reliability of the BFRL

To clarify the repeatability of the experiment results, all three BFRL devices has been measured 10 times. Figure S2a-c shows the lasing spectra obtained from five separate measurements on the three BFRL devices at the same pump power (126 nJ/mm^2). Although, the fluctuation of lasing intensity and modes can be clearly observed, which results from the intrinsic random feature of the BFRL. Such fluctuation is within an acceptable range. The lasing threshold values for the three BFRL devices still show the same tendency (Figure S2d), which means the threshold can be regard as an effective signal for the distinction of the cell types. To further investigate the influence of the different batches of microfluidics and cells, more experiments were carried out. Figure S3 shows the lasing spectra from the three different batches of microfluidics under the same experiment condition. The lasing spectra are slightly different between each other regarding to the spectrum profile. Such spectrum fluctuation is caused by the variation of the laser cavities (i.e. light path loop). The laser cavities are formed by the scattering and reflection provided by the cells and the microfluidics. Either the microfluidic device or the cells were changed, the laser cavities would vary accordingly. The intensity fluctuation arises from the intrinsic properties of random laser (e.g. competition between the laser cavities).[6] However, the main peak positions of the laser spectra

are always same. This is because the main peak positions are determined by the scattering strength of the whole system. Although there might be some random errors that have been introduced to the different microfluidic devices due to the fabrication. Such random errors are normally less than 1 μm (i.e. photolithography precision) and the induced variation of scattering strength can be neglect compared with the whole system. In the case of the sample with different cell batches, the measured laser spectra from the experiments are shown in Figure S4. The results are similar with that using different batches of microfluidics. The reason is also the same. Using different cell batches will only change the laser cavities in the system but not change the scattering strength of the whole system. Thus, the BFRL is still reliable among the samples with different cell and device batches.

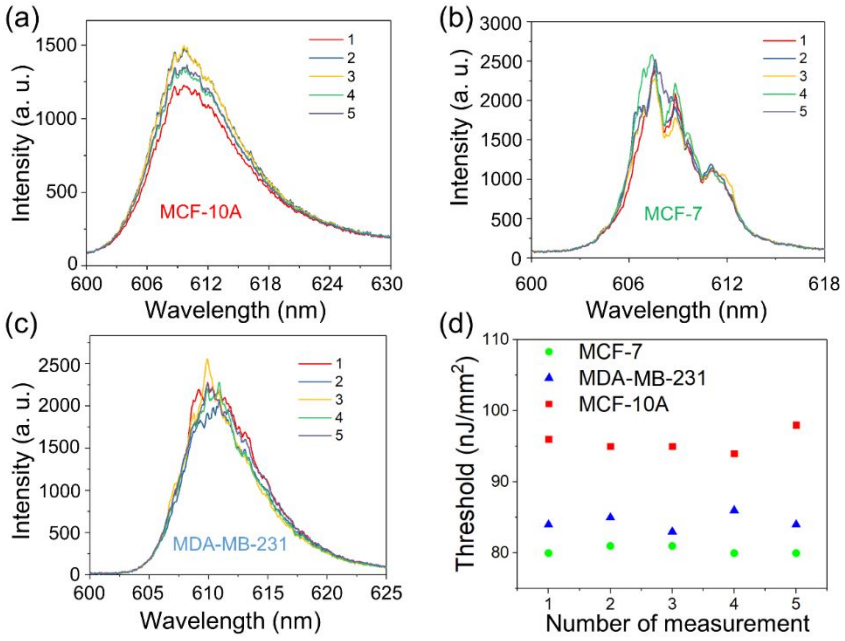

Figure S2. Lasing spectra obtained from five separate measurements on the BFRL filled with (a) MCF-10A, (b) MCF-7 and (c) MDA-MB-231 at the same pump power (126 nJ / mm^2). (d) The calculated lasing threshold values for five separate measurements on the three BFRL devices.

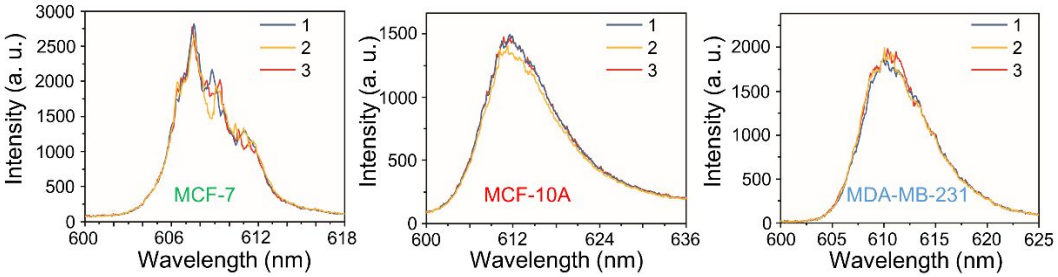

Figure S3. Lasing spectra from the BFRLs built in three different batches of microfluidic device with identical microfluidic design under same experiment condition. Total three microfluidic devices are tested, and the lasing spectra are labeled as batch 1,2,3, respectively. Batch 1 is the result shown in main text.

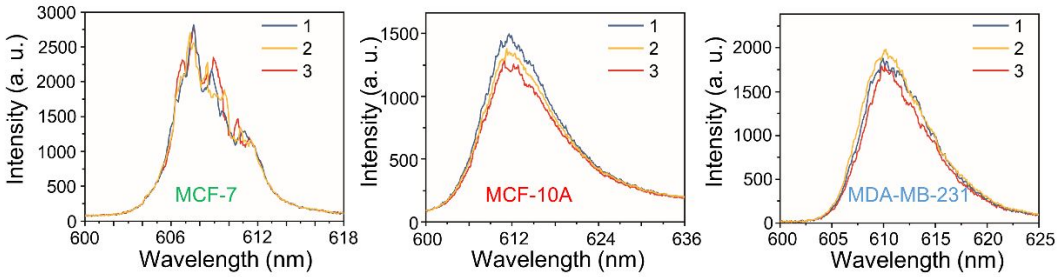

Figure S4. Lasing spectra from the BFRLs with different cell batches under same experiment condition. Total three cell batches are tested, and the lasing spectra are labeled as batch 1,2,3, respectively. batch 1 is the result shown in main text.

Cell type classification and detection of floating cancerous cells using BFRL

Tumor cells are shed into liquid biopsies during the whole carcinoma development. Highly aggressive circulating tumor cells often appears during the later stages of the cancer progressions.[7] Detection of floating cancerous cells in liquid biopsies is one of the core concerns in clinical practices.[8] Biophysical alterations of malignant tumor cells are hallmarks of cancer cells. For example, tumor cells in liquid biopsies tend to be much larger than the normal cells and with higher refractive index.[9] Also, the more malignant tumor cells tend to contain more disrupted cytoskeletons.[10] Considering the BFRL successfully characterized the biophysical properties of the suspended cells, we could use the BFRL properties as the indicators to classify the cells and detect the cancerous cells in a cell mixture.

We firstly determine the most important BFRL properties by principle component analysis (PCA). Three properties (i.e. threshold, peak shift and optical pathlength of fundamental Fourier component $p_{m=1}$) are chosen in the PCA model. PCA delivers linear combinations of the three parameters and the lower-order component dominant the features for classifying the cell types.[11] In our analysis, the first-order principle component is $0.68 \times \text{threshold} + 0.10 \times \text{peak shift} + 0.73 \times \text{optical pathlength}$, in which the optical pathlength is the most important property for cell classification and the threshold comes next. The cell classification result by the first-order and the second-order principle component (indicated by principle component 1 and principle component 2, respectively) is shown in Figure S5a. Using a single indicator of the principle component 1, the three types of cells are successfully classified, as shown in the colored rectangular blocks in Figure S5a. On the other hand, Using the dominant BRFL properties (i.e. threshold and optical pathlength) for cell type classification, we can only classify the three cell types model in a two-dimensional map by using the two properties together, as shown in Figure S5b.

To further validate cancerous cell detection in cell mixtures using BFRL, small amount of cancerous cells (e.g. MFC-7 and MDA-MB-231 cells) are added into MCF-10A suspensions and BFRLs are performed on the mixture suspensions. By using the principle component 1 we introduced in the last paragraph, we successfully identified 5% MCF-7 in cell mixture and 10% MDA-MB-231 in cell mixture, see Figure S5c. Moreover, the MCF-7 and the more invasive cancer cell MDA-MB-231 could be distinguished at an addition of 5%. On the other hand, detection sensitivity by principle component 1 is much higher than using single BFRL properties such as threshold, peak wavelength and optical pathlength (see Figure S6). Thus, the first-order principle component derived by PCA is a good indicator for cancerous cell detection, which provides a potential strategy for random laser bio-sensing.

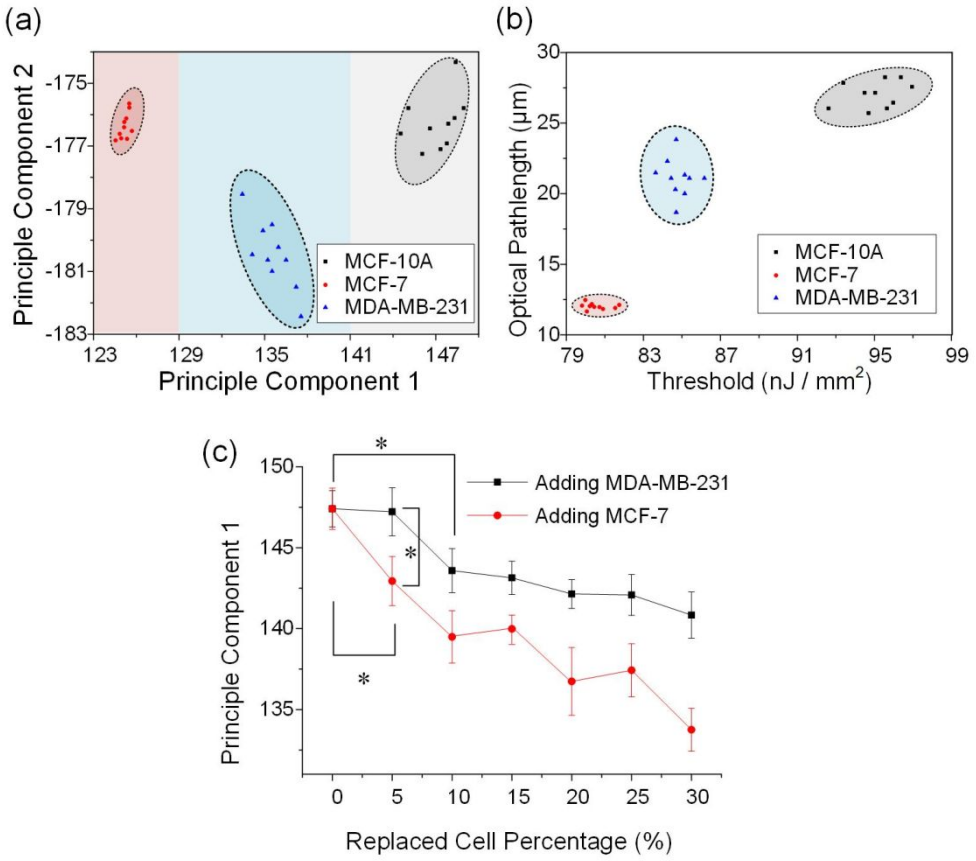

Figure S5. Cell classification and cancer cell detection. (a) principle component analysis for cell type classification (10 measurements for each cell type). The principle component 1 is the first-order component, which equals $0.68 \times \text{threshold} + 0.10 \times \text{peak shift} + 0.73 \times \text{optical pathlength}$, and the principle component 2 is the second order component, which equals $0.71 \times \text{threshold} - 0.37 \times \text{peak shift} - 0.60 \times \text{optical pathlength}$. Using principle component 1 could be capable of classifying the cell types, as indicated by the colored rectangular blocks. (b) cell classification by thresholds and optical pathlength. (c) Detecting cancerous cells in cell mixtures using principle component 1. 5% MCF-7 in MCF-10A could be detected and 10% MDA-MB-231 could be detected. Moreover, MCF-7 and MDA-MB-231 could be distinguished at 5% addition. * indicates statistical significance at a level of 5%.

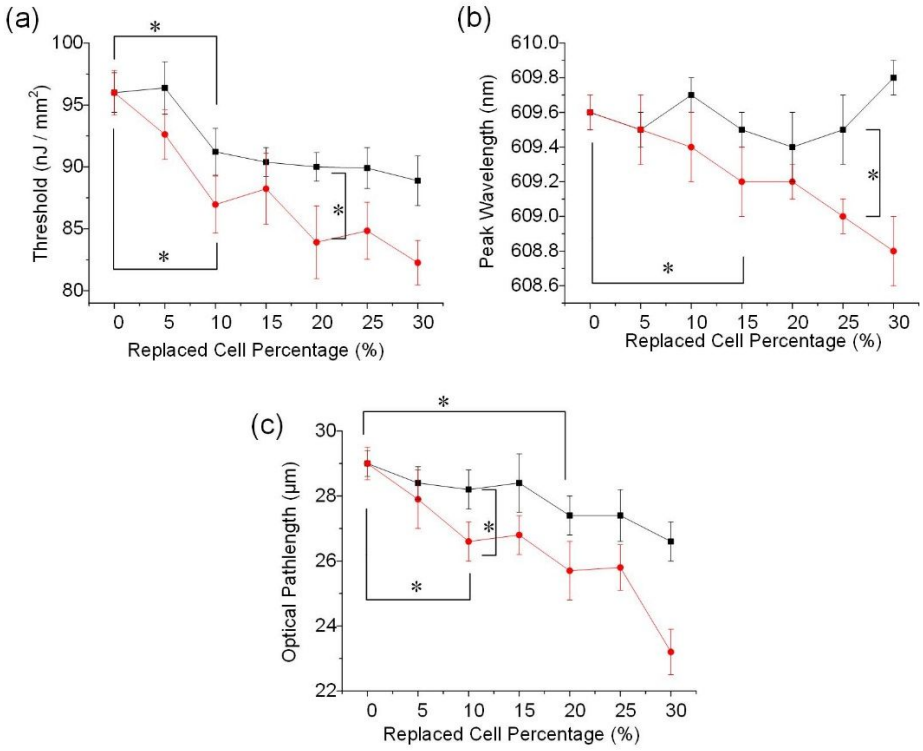

Figure S6. Detecting cancerous cells (MCF-7 and MDA-MB-231) in cell mixtures (in MCF-10A suspensions). (a) Using Threshold as an indicator, 10% MCF-7 in MCF-10A could be detected and 10% MDA-MB-231 could be detected. Moreover, MCF-7 and MDA-MB-231 could be distinguished at 20% addition. (b) Using the peak wavelength as an indicator, 10% MCF-7 in MCF-10A could be detected and MDA-MB-231 could not be detected up to 30%. Moreover, MCF-7 and MDA-MB-231 could be distinguished at 25% addition. (c) Using the peak wavelength as an indicator, 10% MCF-7 in MCF-10A could be detected and 20% MDA-MB-231 could be detected. Moreover, MCF-7 and MDA-MB-231 could be distinguished at 10% addition. * indicates statistic significance at a level of 5%.

References

(1) Liang, X. J.; Liu, A. Q.; Lim, C. S.; Ayi, T. C.; Yap, P. H. Determining Refractive Index of Single Living Cell Using an Integrated Microchip. *Sensors Actuators A Phys.* **2007**, *133* (2), 349–354.

(2) Hsiung, F.; McCollum, T.; Hefner, E.; Rubio, T. Comparisons of Count Reproducibility, Accuracy, and Time to Get Results between a Hemocytometer and the TC20 Automated Cell Counter. *Bulletin* **2013**, *6003*, 1–4.

(3) Wu, X.; Fang, W.; Yamilov, A.; Chabanov, A. A.; Asatryan, A. A.; Botten, L. C.; Cao, H. Random Lasing in Weakly Scattering Systems. *Phys. Rev. A - At. Mol. Opt. Phys.* **2006**, *74* (5), 1–11.

(4) Dice, G. D.; Mujumdar, S.; Elezzabi, A. Y. Plasmonically Enhanced Diffusive and Subdiffusive Metal Nanoparticle-Dye Random Laser. *Appl. Phys. Lett.* **2005**, *86* (13), 1–3.

(5) Meng, X.; Fujita, K.; Murai, S.; Matoba, T.; Tanaka, K. Plasmonically Controlled Lasing Resonance with Metallic-Dielectric Core-Shell Nanoparticles. *Nano Lett.* **2011**, *11* (3), 1374–1378.

(6) Merrill, J. W.; Cao, H.; Dufresne, E. R. Fluctuations and Correlations of Emission from Random Lasers. *Phys. Rev. A - At. Mol. Opt. Phys.* **2016**, *93* (2), 1–5.

(7) Cristofanilli, M.; Budd, G. T.; Ellis, M. J.; Stopeck, A.; Matera, J.; Miller, M. C.; Reuben, J. M.; Doyle, G. V.; Allard, W. J.; Terstappen, L. W. M. M.; et al. Circulating Tumor Cells, Disease Progression, and Survival in Metastatic Breast Cancer. *N. Engl. J. Med.* **2004**, *351* (8), 781–791.

(8) Stott, S. L.; Hsu, C.-H.; Tsukrov, D. I.; Yu, M.; Miyamoto, D. T.; Waltman, B. A.; Rothenberg, S. M.; Shah, A. M.; Smas, M. E.; Korir, G. K.; et al. Isolation of Circulating Tumor Cells Using a Microvortex-Generating Herringbone-Chip. *Proc. Natl. Acad. Sci.* **2010**, *107* (43), 18392–18397.

(9) Liu, P. Y.; Chin, L. K.; Ser, W.; Chen, H. F.; Hsieh, C.-M.; Lee, C.-H.; Sung, K.-B.; Ayi, T. C.; Yap, P. H.; Liedberg, B. Cell Refractive Index for Cell Biology and Disease Diagnosis: Past, Present and Future. *Lab Chip* **2016**, *16* (4), 634–644.

(10) Ketene, A. N.; Schmelz, E. M.; Roberts, P. C.; Agah, M. The Effects of Cancer Progression on the Viscoelasticity of Ovarian Cell Cytoskeleton Structures. *Nanomedicine Nanotechnology, Biol. Med.* **2012**, *8* (1), 93–102.

(11) Abdi, H.; Williams, L. J. Principal Component Analysis. *Wiley Interdiscip. Rev. Comput. Stat.* **2010**, *2* (4), 433–459.